DR MENGKANG FAN (Orcid ID : 0000-0002-8994-6825)

Article type : Regular Paper

Title: Overexpression of the histidine triad nucleotide-binding protein 2 protects cardiac function in the adult mice after acute myocardial infarction

Short title: HINT2 protects cardiac function after acute myocardial infarction

Mengkang Fan[12#], Zhangwei Chen[1#], Yin Huang[3#],Yan Xia[1], Ao Chen[1], Danbo Lu[1], Yuan Wu, Ning Zhang[1], Peipei Zhang[1],Su Li[1], Jinxiang Chen[1], Yingmei Zhang[1], Aijun Sun[1], Yunzeng Zou[1], Kai Hu[1], Juying Qian[1*], Junbo Ge[1*]

[1]Department of Cardiology, Zhongshan Hospital, Fudan University; Shanghai Institute of Cardiovascular Diseases, Shanghai, China

[2]Department of Cardiovascular, Affiliated Hospital of Nantong University, Jiangsu, China

[3] Department of Geriatric Medicine, Affiliated Hospital of Nantong University, Jiangsu, China

# Mengkang Fan, Zhangwei Chen and Yin Huang contributed equally to this article.

* Juying Qian and Junbo Ge are corresponding authors.

Address for Correspondence:

Juying Qian, MD, PhD, FESC, FACC; Department of Cardiology, Zhongshan Hospital, Fudan University, Shanghai Institute of Cardiovascular Diseases, Shanghai, China; 180 Fenglin Road, Shanghai 200032, China; Tel: 86-21-60268565; Fax: 86-21-64223006; Email: qian.juying@zs-hospital.sh.cn

Abstract:

Aim: To explore the role of the histidine triad nucleotide-binding 2 (HINT2) protein in heart failure.

Methods: Neonatal mouse ventricle myocytes (NMVMs) and myocardial infarction-induced heart failure mice were used for *in vitro* or *in vivo* experiments. Adenovirus (ADV) and adeno-associated virus serum type 9 (AAV9) vectors were used to regulate HINT2 expression. The expression of HINT2 was determined by quantifying the mRNA and protein levels. Cell survival was analysed using the CCK-8 kit and TUNEL staining. Mitochondrial function was determined by the mitochondrial membrane potential and oxygen consumption rates. AAV9-HINT2 was injected 24 h post myocardial infarction following which transthoracic echocardiography and histological analyses were performed after 4 weeks. Positron emission tomography tomography-computed tomography (PET/CT) and targeted metabolomics analyses were used to explore the metabolic status *in vivo*. NAD levels were measured using a colorimetric kit. Computer-simulated rigid body molecular docking was performed using AUTODOCK4. Molecule binding kinetics assays were performed using biolayer interferometry.

Results: HINT2 was downregulated in NMVMs in hypoxia. ADV-HINT2-induced HINT2 overexpression improved NMVM survival after exposure to hypoxia. Mitochondrial function was preserved in the ADV-HINT2 group under hypoxic conditions. *In vivo* experiments showed that cardiac function and metabolic status was preserved by HINT2 overexpression. HINT2 overexpression restored mitochondrial NAD levels; this was dependent on nicotinamide mononucleotide(NMN）. Using computer-simulated molecular docking analysis and biolayer interferometry, we observed that HINT2 potentially binds and associates with NMN.

Conclusion: HINT2 overexpression protects cardiac function in adult mice after myocardial infarction by maintaining mitochondrial NAD homeostasis.

KEYWORDS: heart failure, myocardial infarction, mitochondrial function, nicotinamide adenine dinucleotide

1. INTRODUCTION

Heart failure (HF) is the final stage of the majority of heart diseases, such as myocardial infarction (MI), hypertension, and cardiomyopathy [1]. Although there are advanced therapies for HF, the mortality and readmission rate among patients remain high [1]. Some studies have reported a gradual decrease in cellular energy production with the progression of HF [2]. Besides, there is mutual promotion between HF and energy metabolism

dysfunction which finally forms a detrimental positive feedback loop [2, 3]. Therefore, improving energy metabolism in HF is a promising research field.

The histidine triad nucleotide-binding protein 2 (HINT-2) is a member of the HINT family in the HIT superfamily of proteins containing the characteristic HIT motif (His-ϕ-His-His-ϕ-ϕ, where ϕ is a hydrophobic amino acid) [4, 5]. HINT2 is encoded by nuclear gene and is located in hepatocyte mitochondria [5]. Previous studies have shown that it positively regulates energy metabolism. Martin J et al. [6] were the first to report the impaired mitochondrial function resulted in defective lipid metabolism and dysfunctional respiration in HINT2-deficient mice. It is found that the absence of HINT2 changes the acetylation pattern of mitochondrial proteins without affecting the expression of SIRT3,the major deacetylase in mitochondria.. Notably, SIRT3 knockout (KO) mice exhibit similar phenotypes as that of HINT2 KO mice, such as fatty liver, glucose intolerance, and decreased respiration [7, 8]. Interestingly, the deacetylation capacity of SIRT3 was restored in the presence of exogenous nicotinamide adenine dinucleotide (NAD) in HINT2 KO mice [6]. It suggests that HINT2 may affect NAD homeostasis.

NAD is an essential metabolite that participates in multiple pathways. It is a substrate of the NAD-dependent deacetylase and electron carrier in β-oxidation, tricarboxylic acid cycle, and the reactions that lead to ATP production. Preclinical evidence has illustrated that treatment to preserve the NAD pool are beneficial for HF patients. Short-term administration of nicotinamide mononucleotide (NMN), a precursor of NAD, preserves the ultrastructure of mitochondria, reduces reactive oxygen species, prevents cell death in pressure-overloaded hearts, and significantly increases the oxidation of long-chain fatty acids in cardiomyocytes [9]. Stimulating the NAD salvage pathway by overexpressing nicotinamide phosphoribosyltransferase (NAMPT) reduces mitochondrial protein hyperacetylation, alleviates cardiac hypertrophy, and improves cardiac function in response to multiple stresses. Nicolas Diguet et al. [10] confirmed that supplementing nicotinamide riboside stabilizes NAD levels and improves the metabolism of citrate in mice with HF. Previous studies have shown that HINT2 participates in several pathways [11] which are dependent on NAD of existence. However, its function in the heart remains unexplored. Here, we speculate that HINT2 expands the NAD pool thereby showcasing the potential to be used as a therapeutic target for HF.

In this study, we have investigated the protective effect of overexpressing HINT2 in cardiomyocytes and mice with MI and explored the mechanism of HINT2 function in NAD homeostasis. Our work demonstrates that

overexpression of HINT2 is a potential effective therapy to preserve heart function after MI.

2. RESULTS

2.1 HINT2 is down-regulated after hypoxia *in vitro*

As shown in Figure 1A, immunofluorescence experiments showed that HINT2 was expressed in neonatal mouse ventricle myocytes (NMVMs) and reside in the mitochondria. To delineate the role of HINT2, we determined the expression of HINT2 in isolated NMVMs after exposure to hypoxia. Quantitative reverse transcription-polymerase chain reaction (RT-PCR) showed that HINT2 was transcriptionally downregulated (Figure 1B). Immunoblotting results indicated that the protein levels of HINT2 reduced gradually with increased exposure to hypoxia and eventually stabilised after 12 h (Figure 1C, D). The quantitative RT-PCR and immunoblotting results indicated that expression of HINT2 was regulated, at least partially, at the level of transcription. HINT2 was downregulated in hypoxic cardiomyocytes, suggesting that HINT2 plays a unique role in cell survival.

2.2 Overexpression of HINT2 protects NMVMs from hypoxic conditions

The reduced HINT2 protein levels may be an intermediate in cardiomyocytes after being exposed to hypoxia. To explore whether normalized HINT2 could protect cardiomyocytes from hypoxic conditions, we constructed adenoviral (ADV) containing HINT2 gene (ADV-HINT2) or the corresponding shRNA (ADV-shHINT2). Meanwhile ADV containing plasmids without exogenous gene was used as negative control (ADV-NC). The NMVMs were treated with the ADV-HINT2 24 h after they adhered and the transfection efficiency was determined using quantitative RT-PCR and immunoblotting using samples at 36 h after transfection. As shown in Figure 2A–D, HINT2 was successfully overexpressed in NMVMs both at the mRNA and protein levels. Cell viability was measured by the CCK-8 assay. After 12 h of exposure to hypoxia, the viability of NMVMs transfected with ADV-NC significantly reduced by 70% (Figure 2E). Although HINT2 overexpression did not increase the cell viability of NMVMs in normoxic conditions, there was increased cell viability in the ADV-HINT2 cells as compared to the ADV-NC transfected cells under hypoxic conditions. The viability of the NMVMs with ADV-shHINT2 significantly decreased to 43%. TUNEL staining was performed to detect apoptosis in NMVMs. After 12 h of hypoxia, an increased ratio of apoptotic cells were observed in both the ADV-NC and ADV-HINT2 transfected groups. Notably, NMVMs transfected with ADV-HINT2 exhibited a smaller population of apoptotic cells compared to the ADV-NC transfected group (Figure 2F, 2G). Population of

apoptotic NMVMs was significantly increased in with ADV-shHINT2 group compared with ADV-NC group (Figure 2H). These results indicate that HINT2 can protectNMVMs from hypoxia.

2.3 HINT2 preserves mitochondrial function in NMVMs

Mitochondria are the most critical organelles in cardiomyocytes that play a key role in hypoxia-induced cell death and apoptosis. HINT2 is a mitochondrial protein and reduced levels of HINT2 may result in mitochondrial dysfunction. The mitochondrial membrane potential (MMP) plays an essential role in generating mitochondrial energy that largely depends on normal mitochondrial function. To further identify the effects of HINT2 on mitochondrial function, the MMP was determined using laser scanning confocal microscope after incubating with the tetramethylrhodamine methyl ester (TMRM) probe. As shown in Figure 3A and 3B, ADV-shHINT2 reduced MMP compared to NMVMs transfected with ADV-NC. MMP significantly reduced in NMVMs transfected with ADV-NC under hypoxic conditions. Compared to the ADV-NC transfected group, a significantly higher MMP was observed in NMVMs transfected with ADV-HINT2 after exposure to hypoxia (Figure 3C).

To determine the protective role of HINT2 in mitochondrial respiration, NMVMs were transfected with ADV-NC or ADV-HINT2 and the OCR was detected after exposure to hypoxia. The OCR, indicative of mitochondrial function, was detected using SeahorseXF96. As shown in Figure 3D–3F, using the standard glucose curve, the basal OCR decreased by 72.2% and ATP production reduced by 67.9% in NMVMs transfected with ADV-NC after exposure to hypoxia. Upon the addition of the uncoupling agent carbonyl cyanide 4-(trifluoromethoxy) phenylhydrazone (FCCP), the maximum OCR was lowered by 75.3% in the ADV-NC+hypoxia cells as compared to the ADV-NC transfected cells (Figure 3G). Notably, HINT2-overexpressing NMVMs showed lesser reduction in the basal, ATP-linked, and maximum OCRs after hypoxia as compared to the ADV-NC transfected cells (Figure 3E–3H). It indicated that mitochondrial respiration was protected from exposure to hypoxia by the overexpression of HINT2.

2.4 Cardiac-specific HINT2 overexpression preserves cardiac function after MI

Based on the positive effects of HINT2 on mitochondria *in vitro*, we investigated whether HINT2 was beneficial to MI-induced heart in mice. The HINT2 expression profile in MI-induced HF was detected in adult mice using immunoblotting and immunofluorescence. A significant down-regulation of HINT2 was observed in the non-infarct area of LV 4 weeks post MI (Figure 4A–4D). To evaluate the therapeutic efficacy of HINT2 on

failing hearts, we used C57BL/6 male mice with a pre-clinical model of ligated LAD to induce HF. To mimic the treatments as close to the clinical process as possible, genetic therapy was performed post MI. In brief, 5×10^{11} serum type 9 adeno associated virus containing HINT2 gene (AAV9-HINT2) per mouse were administrated via the tail vein injection at 24 h after MI and equivalent negative vectors (AAV9-NC) were used as controls. HINT2 expression was detected after 4 weeks post MI for evaluating the efficacy (Figure 4E–4G).

Cardiac function was determined *in vivo* using transthoracic echocardiography before LAD ligation and at 1 week and 4 weeks after. The cardiac structural and functional dimensions were shown in Table. As shown in Figure 4I, the left ventricular ejection fraction and fractional shortening descending decelerated in mice treated with AAV9-HINT2 at 4 weeks after MI as compared with AAV9-NC. This protective effect of HINT2 expression has been shown in Figure 4J. Pathological analysis was performed 4 weeks after MI to evaluate heart fibrosis using Masson's trichrome staining. We observed that the mice treated with AAV9-HINT2 presented smaller fibrosis regions as compared to the AAV9-NC group (Figure 4K, 4L). As seen in the heart sections, the percentage of TUNEL-positive nuclei significantly reduced in the AAV9-HINT2 group as compared to the AAV9-NC group (Figure 4M, 4N).

2.5 HINT2 overexpression increases the metabolic status in mice with HF

Mitochondrial dysfunction and HF mutually stimulate each other to form a vicious circle. Since HINT2 expression preserved mitochondrial function in cardiomyocytes, we speculated that HINT2 improves cardiac energy metabolism after MI in mice. The positron emission tomography tomography-computed tomography (PET/CT) scan employed fludeoxyglucose (18F-FDG) as a tracer to assess glucose uptake that was able to partially evaluate the metabolic status of the heart *in vivo*. The standard uptake value (SUV) was adjusted with the body weights, radiation doses injected, residual radiation doses, and the duration between the injection and scan. As shown in Figure 5A–5C, both the mean SUV and max SUV decreased in the failing hearts with AAV9-HINT2 or AAV9-NC. Notably, compared to the AAV9-NC group, the mean and max SUV were significantly higher in mice treated with AAV9-HINT2. These results suggested that the HINT2 reduces active region loss and preserves energy metabolism.

Furthermore, metabolomics analysis targeting energy metabolism pathways was performed to investigate the variations in metabolism in LV with HF and HINT2 overexpression. Two hundred substances was screened in this analysis and a total of 183 were relatively quantified. The substances are shown in Figure 5D and statistical

significance was considered when p-value $\leqslant 0.05$ and fold change was more than 1.5 or lower than 0.667 in multiple comparisons. These metabolites were searched in the KEGG database to identify related pathways. To understand the potential biological effect on HF, we analysed the enriched pathways between HF treated with AAV9-NC or AAV9-HINT2. As shown in Figure 5E, the metabolites were mostly enriched in pathways related to purine metabolism, nicotinate and nicotinamide metabolism, oxidative phosphorylation, and the synaptic vesicle cycle. Interestingly, several common metabolites, such as ATP, NAD+, NADH, and NADP were present in most of these pathways.

Based on the comparisons among 4 groups, ATP production significantly decreased in LV tissues with HF that was restored by AAV9-HINT2. Interestingly, the metabolites in the nicotinate and nicotinamide metabolism pathway, such as NAD+ and NADH, were also upregulated in the AAV-HINT2 group with sham or HF (Figure 5F–5H). Since ATP was the downstream molecule in process of generating energy, HINT2 may be more likely to affect the energy metabolism by maintaining the NAD pool.

2.6 HINT2 maintains mitochondrial NAD homeostasis

HINT2 affects mitochondrial energy metabolism by promoting lysine deacetylation of mitochondrial proteins without changing their catalytic activity and expression of SIRT3 [6].To clarify the deacetylation effect of HINT2, overall acetyl-modified proteins in mitochondrial were detected in heart tissues and NMVMs respectively. In failing heart, mitochondrial proteins appeared hyperacetylated, and AAV9-HINT2 treatment reduced the acetylation level (Figure 6A). Besides, a higher level of acetyl-modified mitochondrial proteins was found in NMVMs treated with ADV-shHINT2 compared with control group (Figure 6B). Since SIRT3 mainly localizes to the mitochondria and is a NAD+-dependent deacetylase, HINT2 may regulate deacetylation as a coenzyme or by increasing the levels of the co-substrate. To investigate whether HINT2 elevates the levels of NAD, we determined the NAD+/NADH concentration in NMVMs with or without HINT2 overexpression. As shown in Figure 6C and 6D, although the NAD+/NADH ratio was similar in both the groups, the total NAD pool concentration significantly increased in NMVMs overexpressing HINT2. Notably, ADV-HINT2 also elevated NAD level in mitochondria of NMVMs under hypoxia, but not in cytosol (Figure 6E).

The NAD pool may have been augmented by two main reasons: increased synthesis and decreased degradation. To investigate the primary mechanism of action of HINT2 in increasing the NAD pool, we measured the amounts of the major enzymes involved in the degradation and synthesis of NAD using

immunoblotting. As shown in Figure 6F, the results indicated that the major NAD consumers, SIRT3, PARP-1, and CD38, were not regulated by HINT2, as the enzymes (NAMPT and NMNAT3) for NAD synthesis. The mRNA levels of the members of the SIRT and NMNAT family of proteins were also similar in the ADV-NC and ADV-HINT2 groups (Figure 6G, 6H). It indicates that HINT2 neither reduces NAD+ consumption nor directly influences the expression of the enzymes for NAD synthesis.

In salvage pathway, NAMPT catalyzes nicotinamide to form NMN and then NAD is produced from NMN by NMNAT3 in mitochondrial. To explore the role of HINT2 in NAD synthesis, we used GMX1778 (30 nM; S8117, Selleck, USA) to inhibit catalytic activity of NAMPT, the rate-limited enzyme, and NMN (S5259 , Selleck, USA), a precursor molecules of NAD. As shown in Figure 6GNMN (100 μM) increased NAD levels in NMVMs. However, the amount of NAD in NMVMs treated with ADV-shHINT2 significantly decreased, and exogenous NMN failed to reverse. Furthermore, as shown in Figure 6J, the NAD pool in NMVMs decreased upon treatment withGMX1778, for 12 h, and HINT2 overexpression was failed to compensate this reduction. It indicated that the effect of HINT2 on NAD level was dependent on normal level of NMN. Besides, mitochocronial NAD pool was increased in the presence of exogenous NMN and it was normalized the NAD pool in the NMVMs treated with GMX1778. Interestingly, in the NMVMsco-treated with NMN and ADV-HINT2, the NAD levels were higher compared with the ADV-NC group and this effect was also found at presence of GMX1778 (Figure 6J). These results suggests that HINT2 and NMN are essentially dependent on each other for full functionality.

2.7 HINT2 can bind with NMN

As suggested by the name, HINT2 has a nucleotide binding site. We speculated that the effect of HINT2 may due to intermolecular binding (at least partially). To predict the possibility of this, HINT2 and NMN were analysed via computer simulation using AUTODOCK 4.2.6. As shown in Fig. 7A and 7B, HINT2 and NMN were predicted to bind each other. After using conformation clustering analysis and energy ranking, we found an optimal binding site with the strongest binding energy that had the greatest number of possible conformations.

We performed biolayer interferometry to determine the binding kinetics between NMN and HINT2. As shown in Figure 7C, the signal change exhibited fast association and dissociation between these two molecules, and the signal response was associated with various concentrations of NMN. Most importantly, the fitting examination using a 1:1 model indicated that the kinetics data were reliable (R^2=0.9842).

3. Discussion

The findings in this report demonstrate the downregulation of HINT2 in MI-induced HF. Overexpression of HINT2 alleviated the deteriorated cardiac function and preserved the metabolic status after MI. This effect may be attributed to the maintenance of mitochondrial function and NAD homeostasis in cardiomyocytes, suggesting that HINT2 may be a potential therapeutic target in patients with HF after MI.

Once MI occurs, especially struck in LV, the number of contractions in the heart decreases and LV remodelling progressively aggravates over time. In decompensated HF, metabolism disorder is caused by impaired substrate utilisation and relatively insufficient energy supplements [12]. Even though energy metabolism has been considered as an essential therapeutic direction and researchers has been working on this for decades, there still lacks a well-established treatment plan to preserve the metabolic status in failing hearts. We found that HINT2 expression reduced in cardiomyocytes during hypoxia and tissues of the failing heart, suggesting that HINT2 may play a specific role in response to stress.

Gene therapy based on AAV9 changes target gene expression in specific organs. The serum type 9 AAV is one of the most effective vectors for cardiac-specific expression of target gene [13]. Cardiac-specific AAV9-mediated transgene expression functions within a few days and reaches its maximum in 14 days that remains stable thereafter [14]. Since gene interference using AAV9 has usually been performed prior to MI in previous studies [13], it is not able to distinguish whether the treatment affected the infarct size or alleviated the deterioration of cardiac function. In this study, AAV9 based gene therapy was performed after MI instead of preconditioning the models to mimic patient status. AAV9-HINT2 was administrated to mouse by tail vein injection after MI and HINT2 was stably expressed in HF mouse model, suggesting that cardiac-specific gene therapy is a feasible subsequent treatment for HF after MI.

HINT2 restores metabolism in hepatocytes [6]. This may be partially due to the deacetylation of metabolic enzymes in mitochondria without affecting sirtuin expression. Sirtuins (SIRT1−7), a group of NAD-dependent deacetylases, are enzymes that cleave NAD into nicotinamide and its ADP-ribose moieties to post-translationally modify cellular proteins that regulate metabolism [15]. Among the sirtuins, SIRT3 is the main mitochondrial deacetylase that enhances the activity of the enzymes involved in the Krebs cycle and oxidative phosphorylation [15]. Previous research has shown that SIRT3 protects the heart from pressure overload stress, drug induced cardiotoxicity, and MI [16]. Pillai VB et al.[17] reported that angiotensin 2 and phenylephrine agonists reduce NAD+

concentrations in the heart; the administration of NAD+ alleviates left ventricular hypertrophy in a SIRT3-dependent manner, indicating that the effects of SIRT3 may depend on the normal concentrations of NAD.

Martin J and colleagues [6] reported that HINT2 positively regulates glutamate dehydrogenase activity via deacetylation of proteins without affecting SIRT3 activity. However, this study detected SIRT3 activity in the presence of exogenous NAD+ that could not clarify whether HINT2 regulated NAD+ (a key substrate used during deacetylation). Moreover, a study has reported that HINT2 positively regulates hepatocellular oxidative phosphorylation and associates with GRP75 which binds to the cytochrome c oxidase subunit 4 and promotes the dynamic assembly of the respiratory chain super complexes [11]. In this study, the effect of HINT2 on mitochondrial respiration was confirmed in cardiomyocytes, but we observed that the anti-GRP75 antibody was unable to pull-down HINT2 from the cardiomyocyte lysate (data not shown). Therefore, this mechanism needs to be further explored. NAD+ is a critical coenzyme to produce ATP in mitochondria that participates in the Krebs cycle, electron transport chain, and glucose and fatty acid oxidative phosphorylation as an electron transporter. Thus, a sufficient NAD pool is needed for mitochondrial metabolism. It has been demonstrated that NAD+ levels are rate-limiting in mitochondrial respiration [18]. In this study, HINT2 preserved NAD homeostasis in cardiomyocytes and promoted both deacetylation and mitochondrial respiration. We speculate its effects may be largely due to the regulation of NAD which is shared by both pathways.

Myocardial NAD pools reduced in failing hearts in several mouse models, such as in transverse aorta constriction (TAC) and ischemia reperfusion injury [17, 19]. Studies have shown that the exogenous NAD+ precursor improves NAD levels in the myocardium and preserves heart function in mouse models of HF. In TAC-induced HF mouse models, the NAD pool decreases and short-term administration of NMN successfully protects cardiac mitochondria, reduces cell death, and improves mitochondrial fatty acid oxidation[9]. Another study has drawn similar conclusion that nicotinamide riboside improves citrate metabolism in HF and alleviates the final reduction of left ventricular ejection fraction in the TAC model [19]. In our research, HINT2 restored the mitochondrial NAD pool in the heart tissue which may enable it to perform the therapeutic function.

NAD is synthesized *de novo* from tryptophan or by the Preiss-Handler pathway from nicotinic acid. However, recycling the nicotinamide generated by continuous enzymatic cleavage of NAD within the body depends on the NAD salvage pathway in which NAMPT is the rate-limiting enzyme to produce NMN, a immediate precursor

of NAD.[19]. In Hela cells, NAMPT could not be detected and it was excluded from the mitochondrial matrix. Therefore, the mitochondrial NAD source was more likely to be reliant on supplemented NMN or NAD from the cytosol. NMNAT3 is the downstream molecule of NAMPT that resides in the mitochondria and converts NMN to NAD, whereas the role of NMNAT3 remains controversial. In NMNAT3-deficient mice, NAD levels are normal in the heart, muscle, and liver [20]. Similar conclusions were drawn from other studies that showed NMNAT3 was dispensable for mitochondrial NAD maintenance [12]. Interestingly, in our study, HINT2 increased the NAD pool in the mitochondria of cardiomyocytes without regulating rate-limiting enzymes and main consumers. However, on the one hand, the effect of HINT2 was dependent on the activity of NAMPT or supplementation of NMN in intact cardiomyocytes. On the other hand, when HINT2 was knocked down, the mitochondrial NAD pool decreased and could not be restored by supplementing NMN. It suggests that HINT2 and NMN were both essential for NAD generation, and they neither can increase NAD pool effectively without the other.

In this research, it showed that HINT2 has capacity to bind with NMN, and this structural combination may partially interpret the interaction between HINT2 and NMN. However, the internal mechanism how Although HINT2 can bind NMN, we cannot exclude the existence of other mechanisms to transport NAD into the mitochondria, thus, further experiments are required to delineate potential transporters or pores.

In summary, these results demonstrate that HINT2 preserves heart function and metabolism in the HF mouse model after acute MI, and this beneficial effect may be due to the maintenance of mitochondrial NAD. It suggests that genetics-based therapy can potentially be used to improve the metabolic status after the onset of MI to delay the progression of HF.

4. MATERIALS and METHODS

4.1 Isolating and culturing cells

NMVMs were isolated as described previously with minor modifications [21]. The hearts from 1-day-old C57BL/6 mice were washed and minced in phosphate-buffered saline. Tissues were serially digested with 0.08% collagenase II and incubated at 37°C. The supernatants were transferred into a fresh tube and digestion was terminated upon the addition of equal volumes of Dulbecco's modified Eagle medium containing 10% bovine serum. Subsequently, the cell suspension was centrifuged at 1,000 rpm for 5 min after which the cells were resuspended in the Dulbecco's modified Eagle medium supplemented with 10% bovine serum, 100 U/ml

penicillin, and 100 mg/ml streptomycin. The cells were pre-plated at 37°C for 90 min. After differential adhesion was observed, the cell suspension was diluted to 1×10^6 cells/ml and plated in a culture dish for subsequent experiments. The cells were exposed to hypoxia by transferring them into an anoxic chamber with an atmosphere consisting of 5% CO_2 and 95% N_2.

4.2 Mice and animal procedures

Wild-type C57BL/6 male mice were used for studying MI-induced HF by ligating the left anterior descending branch of the coronary artery (LAD) [22]. All mice were obtained from the Institute of Laboratory Animal Science at Zhongshan Hospital (Shanghai, China). All animal procedures were performed according to the protocols approved by the Animal Care Committee of Zhongshan Hospital. MI was performed on mice that were 6–8 weeks old. Like the previous study, the LAD was ligated under isofluorane anaesthesia without the trachea cannula. Sham surgery was performed using the same procedure (excluding LAD ligation). Adeno-associated virus serum type 9 (AAV9) was injected into the tail vein 24 h after the operation. The person using the injection was well trained and unaware of the grouping process and the mice were randomly divided into the AAV9-NC and AAV9-HINT2 groups to ensure randomization of the AAV9 treatment in each of the mice cohorts. The mice were followed up for 4 weeks after MI and then euthanized. Heart tissues were collected and stored for future experiments.

4.3 Generating plasmids and viral particles

To produce *in vivo* HINT2-overexpressing AAV9, plasmids containing the HINT2 gene were constructed. The expression cassettes were under the control of the cytomegalovirus promoter and contained a SV40 poly(A) chain after the sequence encoding the FLAG peptide. AAV-293 cells were co-transfected with the HINT2 expressing plasmids and those encoding the adenovirus helper functions. The culture media were exchanged 20 hours later with fresh media and the cells were continuously cultured for 72 hours. The AAV9 particles were separated, purified, and their titre were measured before use. To acquire ADVs, the HINT2- or shRNA-HINT2-bearing plasmids were transfected into the HEK293 cells. The ADVs were amplified and collected three times. The ADVs were stored at -80°C. Supplementary Table 1 shows the sequences for the target gene sequences used for constructing the plasmids.

4.4 Cell viability assays

Cell viability was determined using the Cell Counting Kit-8 (C0038, Beyotime, China). NMVMs were seeded in

96-well plates at a concentration of 1×10^4 cells/100 µl/well. After incubating for 24 h, the NMVMs were treated with ADVs for 36 h followed by exposure to hypoxia for 12 h. Following this, 10 µl of CCK-8 was added per well and incubated for 2 h. The absorbance was measured at 450 nm using a microplate reader.

4.5 Determining apoptosis

Apoptosis in vitro was determined by TUNEL staining using Cell Death Detection Kit, TMR red (12156792910 Roche, Switzerland). According to the kit instructions, the cardiomyocytes were fixed and permeated for labelling with dUTP-TMR and the nuclei were stained with DAPI (C1006, Beyotime, China). TUNEL positive cells n the tissue sections were identified using Cell Death Detection Kit, POD (11684817910, Roche, Switzerland) and the nucleus was counterstained using Harris haematoxylin. The cells and tissue sections were observed using the fluorescence and ordinary light microscope, respectively (ZEISS Group, Jena, German). The number of TUNEL-positive and total nuclei were counted in five randomly chosen fields under the 40× objective; the percentage of cells undergoing apoptosis was calculated by dividing TUNEL-positive with total nuclei present.

4.6 Measuring NAD and NADH levels

NAD and NADH levels were determined using the NAD+/NADH Quantification Colorimetric Kit (K337-100, BioVision Inc., USA). The protocol was performed according to the kit instructions. The cells were harvested and lysed using the supplied NADH/NAD Extraction Buffer. A sample solution was used as a pilot test to detect the NADH and total NAD/NADH levels using the NAD Cycling Enzyme Mix. Finally, the absorbance was measured at 450 nm using a microplate reader. The concentration was calculated using the formula obtained from the standard curve. Mitochondria were isolated from the NVNMs using the mitochondria extraction kit (ab110171, abcam, UK). Thereafter, the mitochondrial NAD pool was quantified as per the previously described kit protocol. The protein contents of the samples were determined using the bicinchoninic acid kit (P0012, Beyotime, China) and was used to normalise the NAD/NADH concentration in terms of pmol/mg.

4.7 Measuring OCR

NMVM OCR was determined using the Seahorse XFe96 Analyzer (Seahorse Bioscience, Inc. USA). NMVMs were seeded in the XF96 Cell Culture Microplates at a concentration of 1,000 cells/well and treated as described previously. Culture media were substituted with the base medium containing 10 mM glucose or 1 mM pyruvate, and subsequently, the plates were incubated at 37°C without CO_2 for 1 h. The basal cellular respiration was

quantified following an injection of oligomycin (ATP synthase inhibitor; 1 μM) to measure ATP-linked OCR. An uncoupling agent (FCCP; 0.5 μM) was used to determine maximal respiration. Prior to the test experiments, a titration curve was generated to determine the optimal FCCP concentration that was observed to be 0.5 μM. Rotenone (1 μM) and antimycin A (1 μM) were injected to inhibit complex I and III, respectively and to determine non-mitochondrial respiration. All the plates were treated the same way in triplicates or quadruples, and each experiment was performed at least 3 times. OCR was normalized using the total protein in each well.

4.8 Analysis of MMP

The MMP was detected using the potential-sensitive dye TMRM. Cells were incubated at room temperature in culture media containing 15 nM TMRM. Subsequently, the cultures were observed using confocal microscopy (Olympus, Tokyo, Japan). The laser was used at 543 nm to excite the samples that resulted in an emission from TMRM with a peak at 577 nm. To establish the background fluorescence, 10 μM FCCP was added that completely depolarized mitochondria within a few minutes.

4.9 Transthoracic echocardiography

Transthoracic echocardiography was performed using the Vevo707B instrument (Visual Sonics Inc., Toronto, ON, Canada) to evaluate the function of the left ventricle (LV) [23]. The mice were anesthetized under continuous isoflurane flow at a rate of 1 L/min. The parasternal long-axis view of the LV was used to analyse systolic function; the dimensions, ejection fraction, and fractional shortening of LV were recorded using M-mode imaging.

4.10 PET/CT

To detect the capacity for cardiac glucose uptake, micro-PET/CT analysis was performed 4 weeks after MI. The mice fasted overnight and were anesthetized using 5% isoflurane. The tracker, 18F-FDG (12.12 ± 1.28 Mbq in 100 μl), was injected into the tail vein 45 min before the PET/CT scan (Inveon mPET/CT; Siemens, Knoxville, TN, USA). PET images were aligned with those from the micro-CT for locating the anatomy. Subsequently, the images were reconstructed using three-dimensional ordered subsets expectation-maximization reconstruction. Radiation values were normalized by body weight and injection dosage was calculated using a software considering the maximum standard uptake value and the mean standard uptake value.

4.11 Histology sectioning and analysis

Hearts were harvested and fixed in 4% paraformaldehyde. Tissues were embedded in paraffin and sectioned

from the mid-ventricular region using a slicer. After the heart sections (5 μm) were stained with Masson's trichrome, the infarct size and fibrotic lengths were calculated as the average ratio of scar length to total LV circumference using the ImageJ software (National Institutes of Health, Bethesda, MD, USA).

4.12 Quantitative RT-PCR

Total RNA was extracted from the mice heart tissues and NMVMs using TRIzol according to the instructions provided. Primers for reverse transcription have been shown in Supplementary Table 2.

cDNAs were generated from the RNAs using the First Strand cDNA Synthesis Kit for quantitative RT-PCR (Takara, Tokyo, Japan) with the cycling conditions of 37°C for 15 min followed by 85°C for 5 s and 4°C for 5 min with the T100 Thermal Cycler (Bio-rad Laboratories Inc., USA). Quantitative real-time PCR was performed using the CFX Connect Real-Time System (Bio-rad Laboratories Inc., USA) in 10 μl reactions comprising 50 ng cDNA, 0.2 μM primers, and 5 μl Master SYBR Green I (Takara, Japan). Data from the quantitative real-time PCR were analysed using the $2^{-\Delta\Delta CT}$ method as described by Livak and Schmittgen [24]. The sequences of the primers used in these experiments are shown in Supplementary Table S1. Expression of the proteins were normalized using the levels of β-actin. The amplification conditions used were 39 cycles of denaturation at 95°C for 30 s followed by annealing and extension at 60°C for 30 s.

4.13 Immunoblotting and immunofluorescence

Immunoblotting and immunofluorescence was performed as described previously using the primary antibodies as follows: Anti-HINT2 (AT5B10, NOVUS biologicals Inc., USA); anti-PARP-1 (#9532, Cell Signaling Technology, USA); Anti-acetylated-lysine(#9441 Cell Signaling Technology, USA) Anti-CD38 (ab216343, Abcam, UK); Anti-acetylated-lysine (#9441, Cell Signaling Technology, USA); Anti-PBEF (A300-372A, Bethyl Laboratories, USA); Anti-SIRT3 (sc-365175, Santa Cruz, USA; Anti-Sirt5 (#8779, Cell Signaling Technology, USA); Anti-NMNAT3 (sc390433, Santa Cruz, USA); Anti-NMNAT2 (sc-515206, Santa Cruz, USA); Anti-rabbit (#7074, Cell Signaling Technology, USA); Anti-mouse (#7076, Cell Signaling Technology, USA); and Anti-FLAG (F7425, Sigma-Aldrich, USA).

4.14 Targeted metabolomics analysis

High throughput targeted metabolomics was performed as described by Cai Y et al. [25]. In this study, the analysis of the targeted metabolomics was based on high performance liquid chromatography/mass spectrometry targeting 200 common energy metabolites. The tissues were suspended in buffer containing methyl alcohol,

acetonitrile, and water (in a ratio of 2:2:1). The protein precipitates was quantified using bicinchoninic acid to analyse the relative quality of the samples. After dissolution into 50% acetonitrile, the samples were centrifuged and the supernatant was injected into the Agilent 1209 HPLC system (Agilent Technologies, USA). Subsequently, mass spectrum analysis was performed by the Agilent 6460 QqQ Analyzer (Agilent Technologies, USA). The data was extracted using the MRM Analyzer as described previously [25]. All the samples were mixed to determine their qualities and the relative standard deviation (lower than 30%) were considered reliable. The consumables and reagents used were as follows: the ACQUITY UPLC BEH Amide 1.7 μm × 2.1 mm × 100 mm column; acetonitrile (1499230-935, Merck, Genmany); methyl alcohol (144282,Merck, Genmany); methanoic acid 06450 (Fluka,Switzerland); ammonium acetate (70221, Sigma-Aldrich, USA); and all the 200 standards of candidate metabolites were purchased from Sigma-Aldrich.

4.15 Ligand docking and binding site prediction

Computer simulations for molecular docking was performed using AUTODOCK 4.2.6 [26]. The 3D structure of the human HINT2 protein and NMN were obtained from the PDB and Pubchem databases, respectively. Rigid docking was performed using HINT2 and NMN as the receptor and ligand, respectively. The binding capacity was evaluated using the binding energy and inhibitor constant. Clustering analysis using root-mean-square deviation was performed to identify the optimal binding conformation.

4.16 Molecular binding kinetics assay

We constructed a prokaryotic expression vector containing human HINT2. After expression and purification, the recombinant human HINT2 protein with a HIS-tag was obtained at a final concentration of 1.5 mg/ml. A binding kinetics assay was performed between molecules using biolayer interferometry with the Octet Red96 system (ForteBio Inc., USA) [27]. Ni-NTA biosensors (ForteBio Inc., USA) were loaded with the recombinant human HINT2 protein and transferred into buffers containing 0.5 M gradient-diluted NMN (S5259, Selleck, USA) and ddH2O for the association and dissociation kinetics assay. Signals were recorded for processing the data and all data were analysed using Fortebio data analysis 9.0 for calculating the constants and response. Fitting examination was performed with a 1:1 model and goodness of fit (R^2) was used to evaluate the reliability of the data.

4.17 Statistical analysis

In this study, data with continuous variables were presented as mean ± standard deviation. Student's *t*-test was

used to compare between two groups. One-way analysis of variance was used to determine statistical significance in more than two groups and Tukey's post hoc test was used for multiple comparisons. All analyses were performed using GraphPad Prism Software Version 7. $P<0.05$ was considered statistically significant.

ACKNOWLEDGEMENTS

This study was funded by grants from the National Natural Science Foundation of China (Grant Nos: 81970295, 81870267, 81670318, 81900307, and 81570314), Shanghai Municipal Commission of Health and Family Planning (Grant No: 2017YQ057), Shanghai Science and Technology Committee (Grant No: 17411962300), National Program on Key Basic Research Project of China (973 Program; Grant No: 2014CBA02003), Zhongshan Hospital Affiliated to Fudan University (Grant No: 2018ZSLC01, 2015ZSYXGG07 and 2017ZSYQ08), VG Funding of Clinical Trials (2017-CCA-VG-036), Merck (Xinxin-merck-fund-051), and Program for Outstanding Medical Academic Leader (Grant No: 2015-Weijiwei-24).

CONFLICT OF INTEREST

The authors declare no conflicts of interest.

References

1. Ponikowski P, Voors AA, Anker SD, et al.2016 ESC Guidelines for the diagnosis and treatment of acute and chronic heart failure: The Task Force for the diagnosis and treatment of acute and chronic heart failure of the European Society of Cardiology (ESC). Developed with the special contribution of the Heart Failure Association (HFA) of the ESC. *Eur J Heart Fail*. 2016;8:891-975.
2. Schilling J, Kelly DP.The PGC-1 cascade as a therapeutic target for heart failure. *J Mol Cell Cardiol*. 2011;4:578-83.
3. Sheeran FL, Pepe S.Mitochondrial Bioenergetics and Dysfunction in Failing Heart. *Adv Exp Med Biol*. 2017;65-80.
4. Maize KM, Wagner CR, Finzel BC.Structural characterization of human histidine triad nucleotide-binding protein 2, a member of the histidine triad superfamily. *FEBS J*. 2013;14:3389-98.
5. Martin J, Magnino F, Schmidt K, et al.Hint2, a mitochondrial apoptotic sensitizer down-regulated in hepatocellular carcinoma. *Gastroenterology*. 2006;7:2179-88.
6. Martin J, Maurhofer O, Bellance N, et al.Disruption of the histidine triad nucleotide-binding hint2 gene in mice affects glycemic control and mitochondrial function. *Hepatology*. 2013;5:2037-48.
7. Hirschey MD, Shimazu T, Goetzman E, et al.SIRT3 regulates mitochondrial fatty-acid oxidation by reversible enzyme

deacetylation. *Nature*. 2010;7285:121-5.

8. Kendrick AA, Choudhury M, Rahman SM, et al.Fatty liver is associated with reduced SIRT3 activity and mitochondrial protein hyperacetylation. *Biochem J*. 2011;3:505-14.
9. Zhang R, Shen Y, Zhou L, et al.Short-term administration of Nicotinamide Mononucleotide preserves cardiac mitochondrial homeostasis and prevents heart failure. *J Mol Cell Cardiol*. 2017;64-73.
10. Diguet N, SAJ T, Tannous C, et al.Nicotinamide Riboside Preserves Cardiac Function in a Mouse Model of Dilated Cardiomyopathy. *Circulation*. 2018;21:2256-2273.
11. Rajasekaran R, Felser A, Nuoffer JM, et al.The histidine triad nucleotide-binding protein 2 (HINT-2) positively regulates hepatocellular energy metabolism. *FASEB J*. 2018;fj201701429R.
12. Doenst T, Nguyen TD, Abel ED.Cardiac metabolism in heart failure: implications beyond ATP production. *Circ Res*. 2013;6:709-24.
13. Bär C, de Jesus B B, Serrano R, et al.Telomerase expression confers cardioprotection in the adult mouse heart after acute myocardial infarction. *Nat Commun*. 2014;5863.
14. Konkalmatt PR, Beyers RJ, O'Connor DM, et al.Cardiac-selective expression of extracellular superoxide dismutase after systemic injection of adeno-associated virus 9 protects the heart against post-myocardial infarction left ventricular remodeling. *Circ Cardiovasc Imaging*. 2013;3:478-86.
15. Cencioni C, Spallotta F, Mai A, et al.Sirtuin function in aging heart and vessels. *J Mol Cell Cardiol*. 2015;55-61.
16. Sundaresan NR, Gupta M, Kim G, et al.Sirt3 blocks the cardiac hypertrophic response by augmenting Foxo3a-dependent antioxidant defense mechanisms in mice. *J Clin Invest*. 2009;9:2758-71.
17. Pillai JB, Isbatan A, Imai S, Gupta MP.Poly(ADP-ribose) polymerase-1-dependent cardiac myocyte cell death during heart failure is mediated by NAD+ depletion and reduced Sir2alpha deacetylase activity. *J Biol Chem*. 2005;52:43121-30.
18. Bai P, Cantó C, Oudart H, et al.PARP-1 inhibition increases mitochondrial metabolism through SIRT1 activation. *Cell Metab*. 2011;4:461-468.
19. Hsu CP, Oka S, Shao D, et al.Nicotinamide phosphoribosyltransferase regulates cell survival through NAD+ synthesis in cardiac myocytes. *Circ Res*. 2009;5:481-91.
20. Hikosaka K, Ikutani M, Shito M, et al.Deficiency of nicotinamide mononucleotide adenylyltransferase 3 (nmnat3) causes hemolytic anemia by altering the glycolytic flow in mature erythrocytes. *J Biol Chem*. 2014;21:14796-811.
21. Wang K, Long B, Zhou LY, et al.CARL lncRNA inhibits anoxia-induced mitochondrial fission and apoptosis in

cardiomyocytes by impairing miR-539-dependent PHB2 downregulation. *Nat Commun*. 2014;3596.

22. Gao E, Lei YH, Shang X, et al.A novel and efficient model of coronary artery ligation and myocardial infarction in the mouse. *Circ Res*. 2010;12:1445-53.
23. Chen A, Chen Z, Xia Y, et al.Proteomics Analysis of Myocardial Tissues in a Mouse Model of Coronary Microembolization. *Front Physiol*. 2018;1318.
24. Livak KJ, Schmittgen TD.Analysis of relative gene expression data using real-time quantitative PCR and the 2(-Delta Delta C(T)) Method. *Methods*. 2001;4:402-8.
25. Cai Y, Kai W, Guo Y, et al.An integrated targeted metabolomic platform for high-throughput metabolite profiling and automated data processing. 2015;-.
26. Seeliger D, de Groot BL.Ligand docking and binding site analysis with PyMOL and Autodock/Vina. *J Comput Aided Mol Des*. 2010;5:417-22.
27. Abdiche Y, Malashock D, Pinkerton A, Pons J.Determining kinetics and affinities of protein interactions using a parallel real-time label-free biosensor, the Octet. *Anal Biochem*. 2008;2:209-17.

Table Structural and functional dimensions from transthoracic echocardiography detection

		SHAM n=8	SHAM+AAV9-HINT2 n=8	HF+AAV9-NC n=8	HF+AAV-HINT2 n=8
LVEF(%)	Baseline	70.35±5.21	73.87±7.01	68.21±4.58	71.73±2.73
	1w	75.26±7.01	70.54±4.21	49.75±7.45	48.75±14.51
	4w	67.99±8.21	69.20±9.75	27.44±9.55	42.61±11.89
FS(%)	Baseline	39.22±4.09	41.92±6.18	36.99±3.82	38.24±4.12
	1w	43.42±6.53	39.89±4.12	24.75±4.42	24.64±8.52
	4w	38.40±12.89	39.24±13.51	13.47±5.92	20.33±5.72
LVESV(μl)	Baseline	16.39±5.36	12.26±5.37	15.39±3.75	15.92±3.78
	1w	14.12±2.01	14.37±2.48	25.94±5.09	29.19±12.90
	4w	23.24±8.55	17.55±3.12	103.40±58.07	70.84±44.59
LVEDV(μl)	Baseline	54.27±9.37	46.28±10.52	54.64±8.52	52.70±6.37
	1w	53.47±6.71	50.85±5.89	51.76±8.16	54.83±9.07
	4w	63.62±10.33	62.75±12.65	140.02±56.92	113.06±51.19

LVEF, Left ventricular ejection transfusion; FS, fractional shortening; LVESV, left ventricular end systolic volume; LVEDV, left ventricular end diastolic volume.

Figure legends:

Figure 1. The expression of HINT2 in NMVMs. (A) Immunocytochemistry for Hint2 in NMVMs. Cell nuclei (in blue, Scale bar = 10μm), Hint2 (in green) and the mitochondrial marker (in red) as shown in the overlay (in yellow). (B) HINT2 gene expression under hypoxia for 12h by quantitative RT-PCR. (C, D) Expression of Hint2 protein of NMVMs in different duration of hypoxia by immunoblotting with antibody against HINT2. (n=5 different fields; Statistical significance between 2 groups was determined by the 2-tailed unpaired Student's *t*-test, and among groups it was determined by ANOVA with Tukey post hoc tests.*$P< 0.05$, †$P<0.01$, ‡$P<0.001$, for statistical analyses, at least three independent experiments were performed)

Figure2. HINT2 protects NMVMs from hypoxia. (A-D) Expression of HINT2 in NMVMs after transfection of ADV-HINT2 or ADV-shHINT2 by quantitative RT-PCR and immunoblotting. (E) Effect of HINT2 on cell viability after 12h hypoxia stimuli by CCK8 analysis. (F, G). Effect of HINT2 overexpression on hypoxia induced cell apoptosis. TUNEL (in red, left panel) and DAPI (in blue, middle panel) stained nucleus was shown in the overlay (in violet, right panel). (H) Effect of reduced HINT2 expression on proportion of cell apoptosis. (n=5 different field, Scale bar=100μm; Statistical significance between 2 groups was determined by the 2-tailed unpaired Student's *t*-test, and among groups it was determined by ANOVA with Tukey post hoc tests. *$P< 0.05$, †$P<0.01$, ‡$P<0.001$)

Figure3. HINT2 preserves the mitochondrial function of NMVMs. (A) Representative image of effect of ADV-shHINT2 on MMP. Fluorescent properties recorded by confocal microscopy, after NMVMs were labeled with TMRM, a MMP tracker. (B, C) Effect of ADV-shHINT2 and ADV-HINT2 on MMP shown as ratio of the fluorescence intensity before and after FCCP treatment (F/F0). (D) The effect of HINT2 on OCR of NMVMs after hypoxia stimuli. OCR was measured by Seahorse XF96 analyses and normalized to protein levels. Glucose (10 mM) and glutamine (1 mM) served as substrates. (Values are means ± SD of 3 independent experiments with 8 replicates). The OCR profile was measured after sequential additions of A↓ oligomycin (1 mM), B↓ FCCP (0.75 mM), and C↓ antimycin and rotenone (1 mM). (E) Basal respiration; (F) ATP production; (G) Maximal respiration. (H) Spare respiratory capacity. (Statistical significance between 2 groups was determined by the 2-tailed unpaired Student's *t*-test, and among groups it was determined by ANOVA with Tukey post hoc

tests. *P< 0.05, †P＜0.01, ‡P＜0.001)

Figure4. Cardiac-specific HINT2 overexpression preserves cardiac function after MI. (A,B) Expression of HINT2 in failing heart by immunofluorescence. (Scale bar=100 μm) (C, D) Expression of HINT2 protein in heart tissue treated with AAV-HINT2 by immunoblotting using anti-HINT2 antibody. (E) Representative image of efficiency of AAV9-HINT2-Flag in heart tissues. Expression of target gene in LV tissue section by co-immunostaining with anti-Flag (in red) and anti-cTnT (in green) antibodies to identify infected cardiomyocytes. Cell nuclei were stained with DAPI (in blue). (Scale bar 50 μm) (F, G) Expression of HINT2 in failing heart tissues by immunoblotting. (H) Representative M-mode echocardiograms for each group at 4 weeks post MI. (I, J) LVEF and FS at 1 and 4 weeks in mice treated using AAV9-NC or AAV9-HINT2. (K) Representative Masson's trichrome staining of transverse heart sections of each group, SHAM+ADV-NC (upper left), SHAM+ADV-HINT2(upper right), HF+ADV-NC (left bottom) and HF+ADV-HINT2(right bottom). (Scale bar= 1mm). (L) Fibrotic area relative to total LV area shown as mean ± SD. (M) Representative images of cell apoptosis detected in heart sections by TUNEL staining (brown). Cell nuclei were stained with Harris hematoxylin (blue) (Scale bar= 100μm). (N) Percent of TUNEL positive cells in each group (n=8, Statistical significance between 2 groups was determined by the 2-tailed unpaired Student's *t*-test, and among groups it was determined by ANOVA with Tukey post hoc tests.*P < 0.05, *P< 0.05, †P＜0.01, ‡P＜0.001)

Figure5. HINT2 overexpression improves myocardial metabolism status. (A) Representative images of myocardial glucose uptake, determined by micro-PET using 18F-FDG. (B, C) Myocardial glucose uptake SUVmax and SUVmean for three groups of mice. SUV was normalized to the total amount of radioisotope injected and the body weight of mice. Values are expressed as mean±SD (n =5-6 per group). Effect of HINT2 overexpression on metabolites in energy metabolism pathway by high throughput targeted metabolomics analysis. (D) Heat map of the metabolites with p value ≤ 0.05 and the difference of FC value was more than 1.5 or lower than 0.667 in multiple comparisons. (E) The major pathways with containing differential metabolites between HF+AAV9-NC and HF+AAV9-HINT2 group by the KEGG enrichment pathway analysis. (F-H) Relative quantification of major concerned metabolites, NAD, NADH and ATP was shown as median with min to max. (n=4, Statistical significance among groups it was determined by ANOVA with Tukey post hoc tests.

*P< 0.05, †P＜0.01, ‡P＜0.001)

Figure6. HINT2 maintains mitochondrial NAD pool homeostasis in vitro. (A) Effect of overexpression of HINT2 on overall mitochondrial acetylated protein in heart tissues among mice with HF. (B) Acetylation of of mitochondrial protein in NMVMs treated with or without ADV-shHINT2. (C) Effect of HINT2 overexpression on ratio of NAD+/NADH in NMVMs. (D) Effect of HINT2 on NAD+, NADH and total NAD. (E) HINT2 increased mitochondrial NAD rather than cytosol with or without hypoxia stimuli. (F) Effect of ADV-HINT2 on expression of major proteins in pathways of NAD synthesis and consumption by immunoblotting. (G, H) Expression of potential related genes in response to overexpression of HINT2 by quantitative RT-PCR. (I, J) Mitochondrial NAD pool in NMVMs with various treatments. NMN, a NAD precursor, and GMX1778, an inhibitor of NAMPT were used to clarify effective target of HINT2. (n=6-8, Statistical significance between 2 groups was determined by the 2-tailed unpaired Student's *t*-test, and among groups it was determined by ANOVA with Tukey post hoc tests. *P< 0.05, †P＜0.01, ‡P＜0.001) .

Figure7. HINT2 have the binding site and capacity to associate with NMN. (A) Recluster analysis for seeking optimal conformation with computational docking (RMSD=4.0); (B) The strongest binding conformation predicted by computation (left panel) and its related parameters, binding energy, inhibit constant and site of hydrogen bonds (right panel). The energy of each hydrogen bond was shown between the 3D structures of HINT2 and NMN (kcal/mol). (C) Molecules binding kinetics between HINT2 and NMN. (R^2=0.9842)

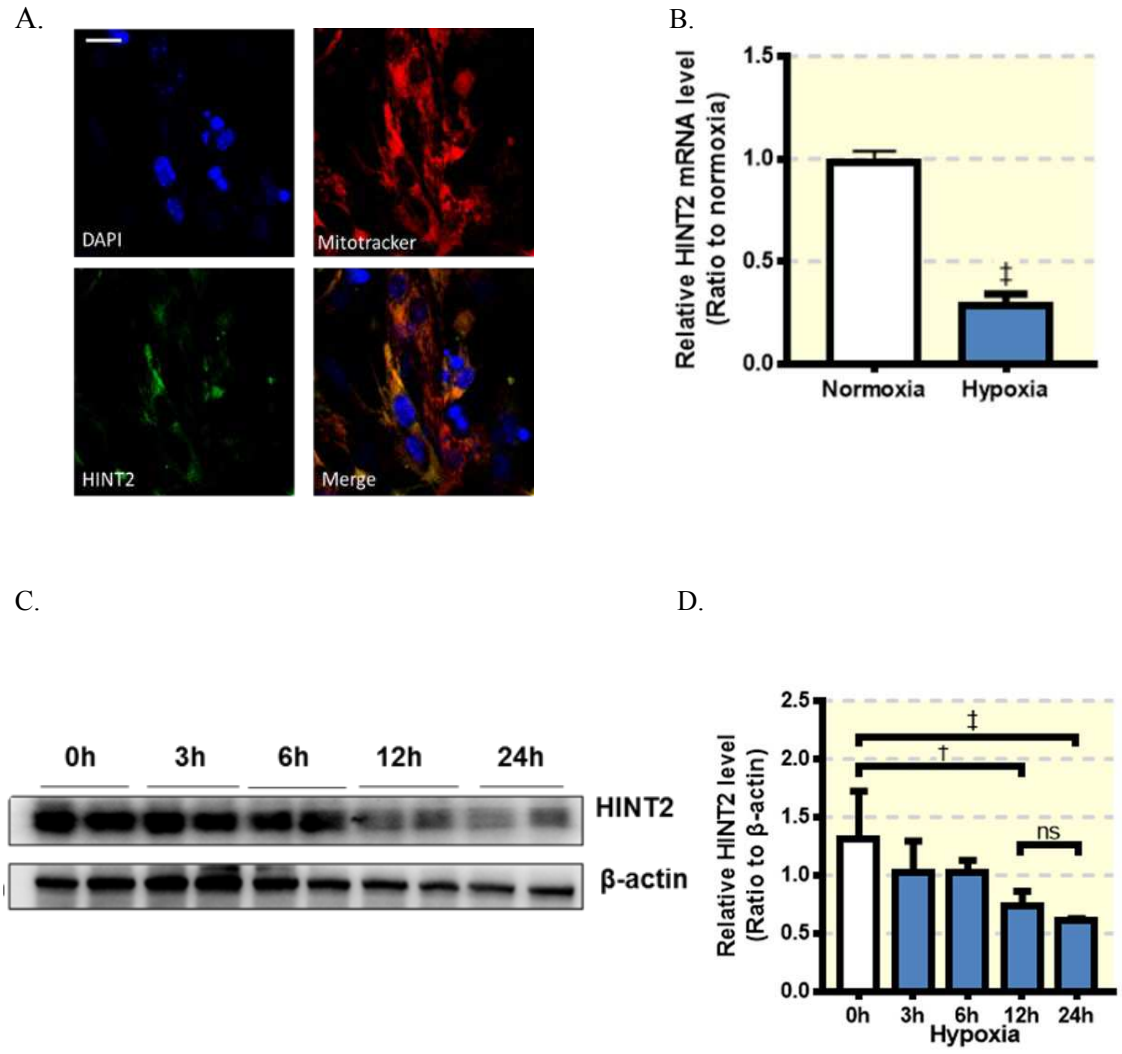

Figure 1

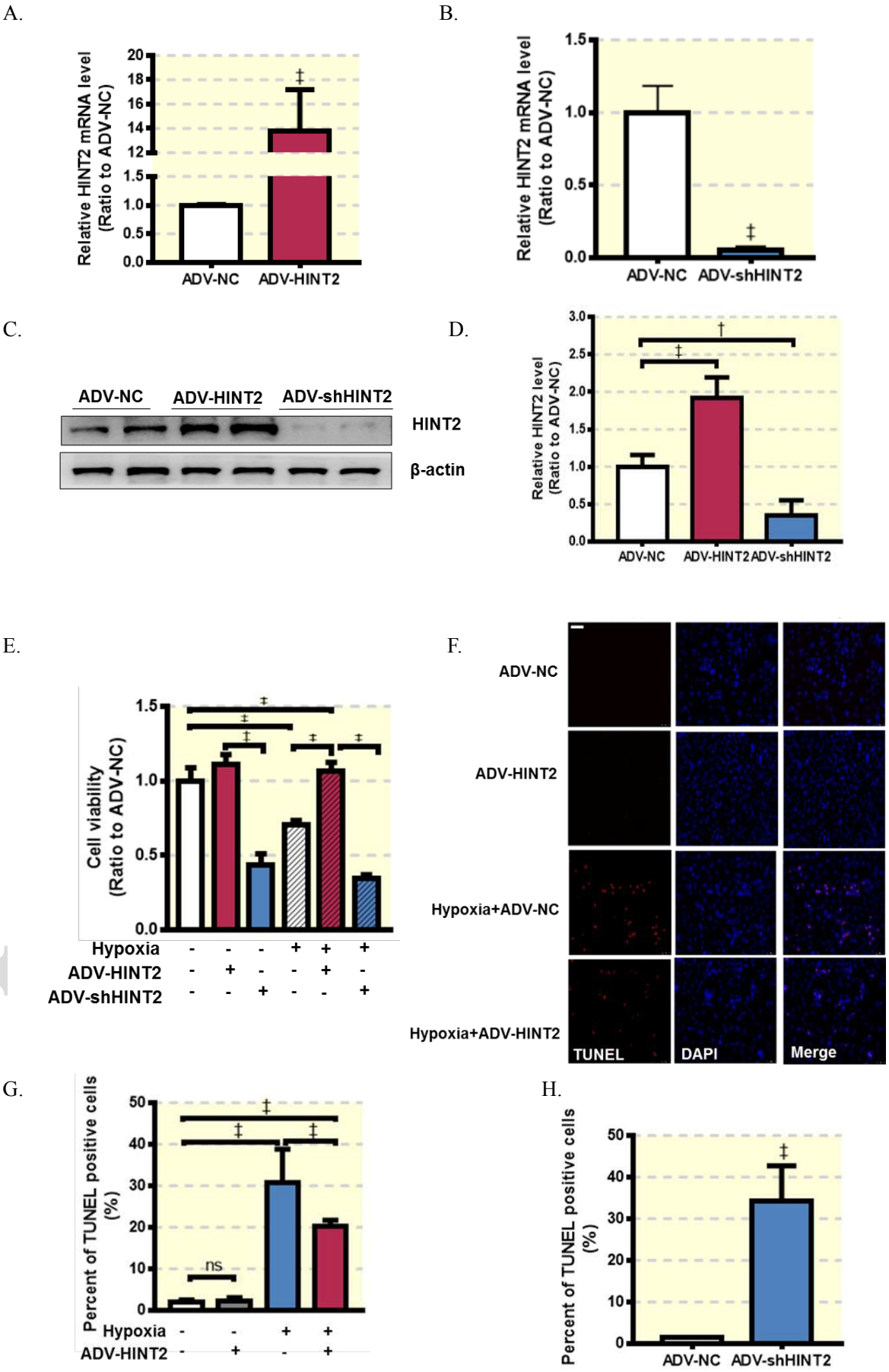

Figure 2

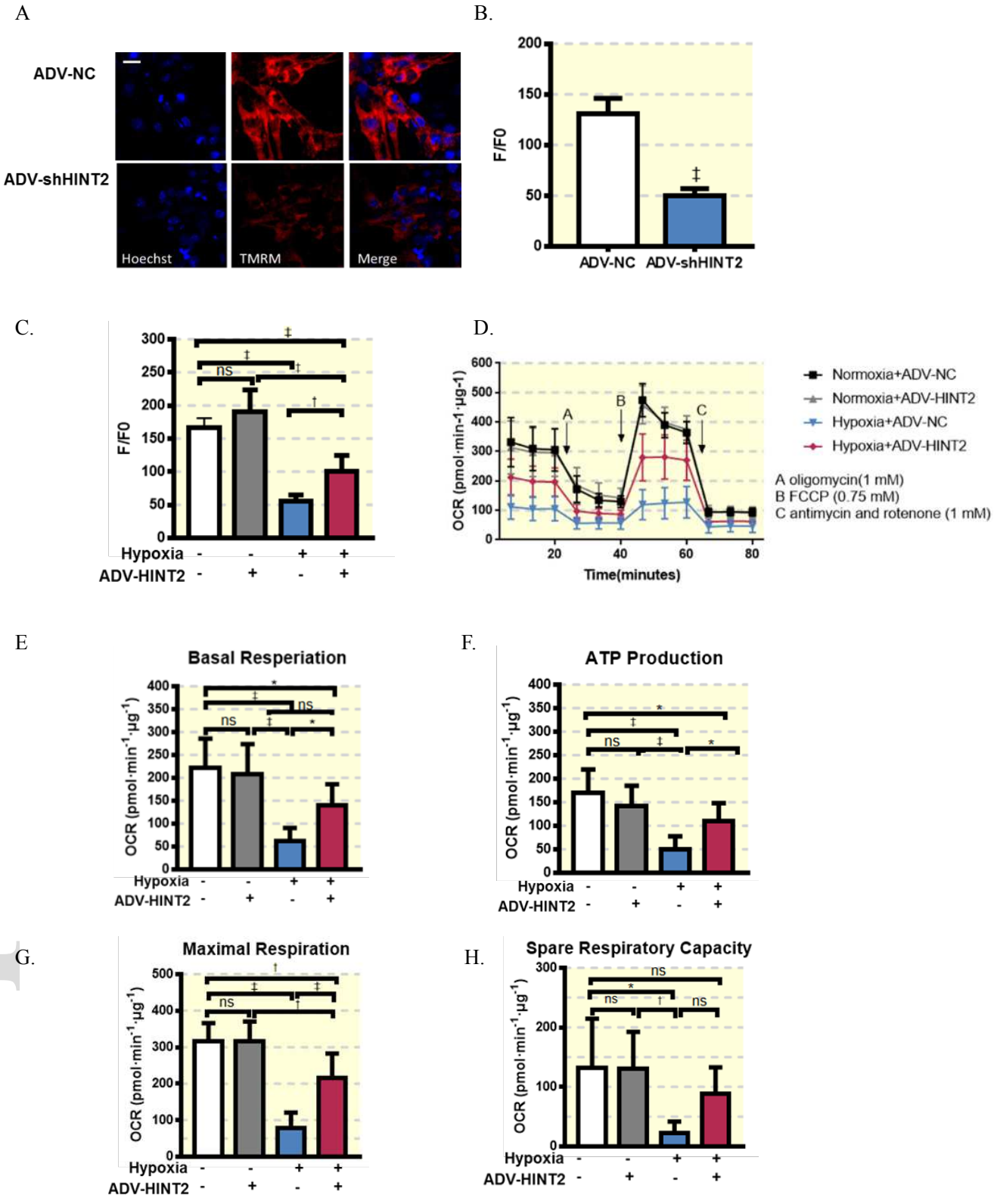

Figure 3

A

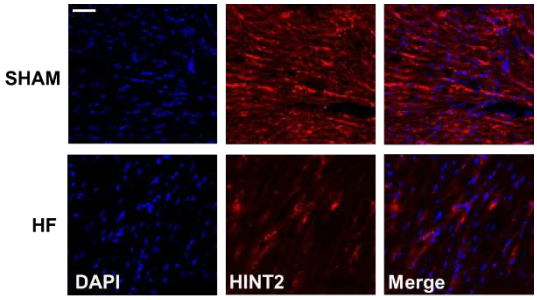

B.

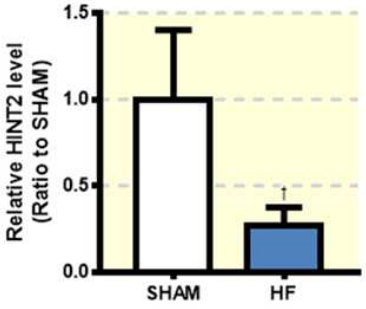

C.

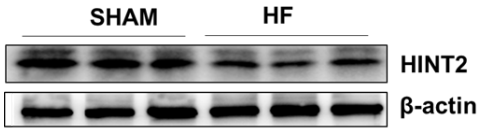

D

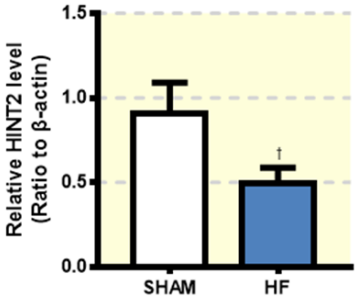

E

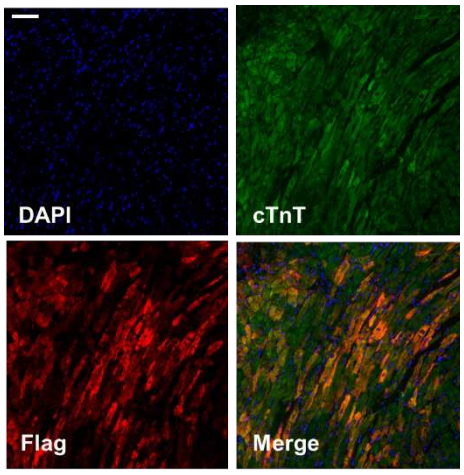

F

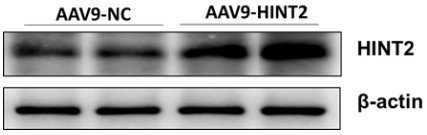

G

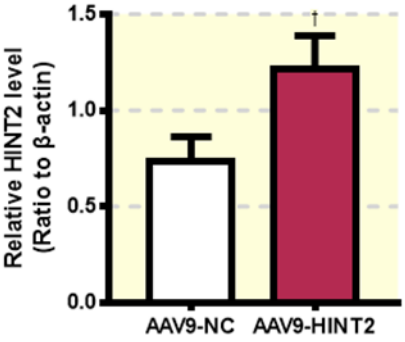

H

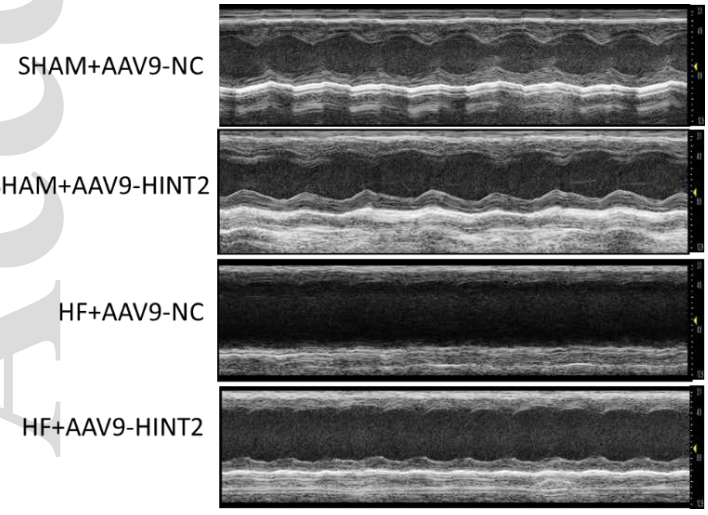

I

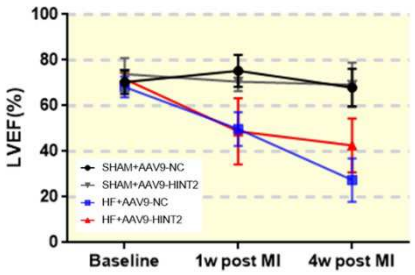

J

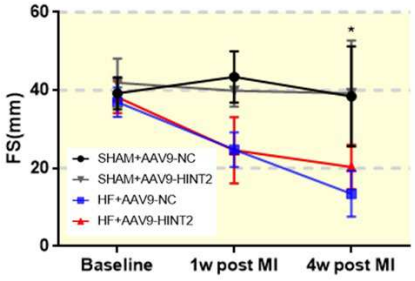

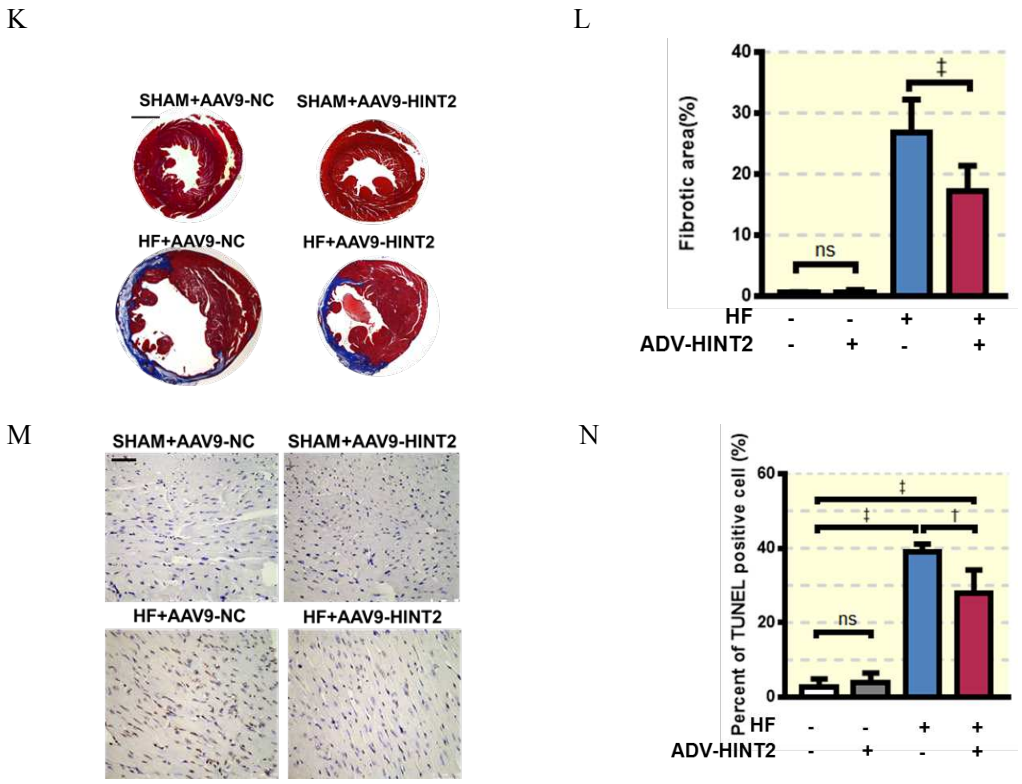

Figure 4

A

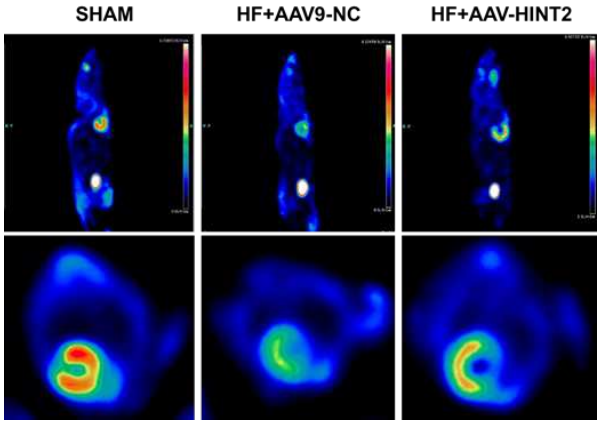

B

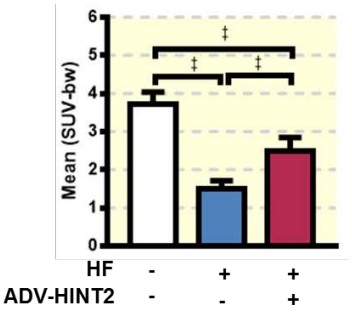

C

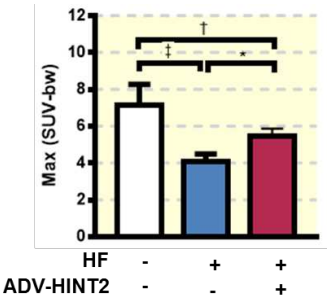

D

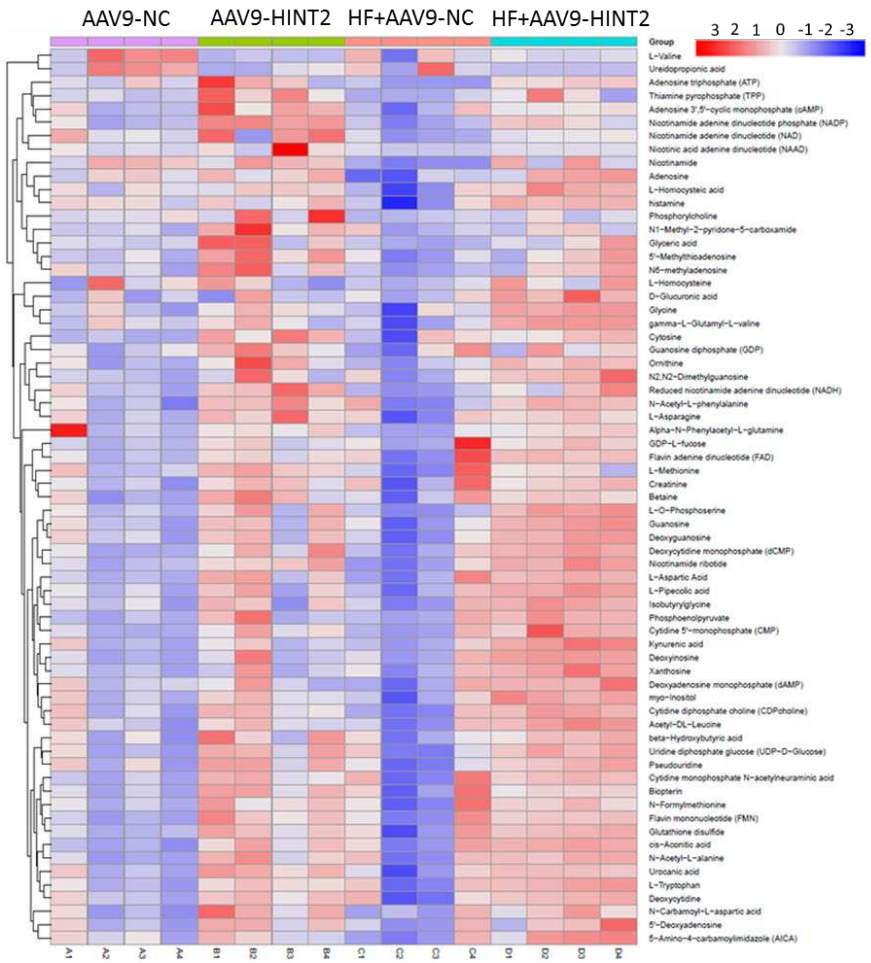

E

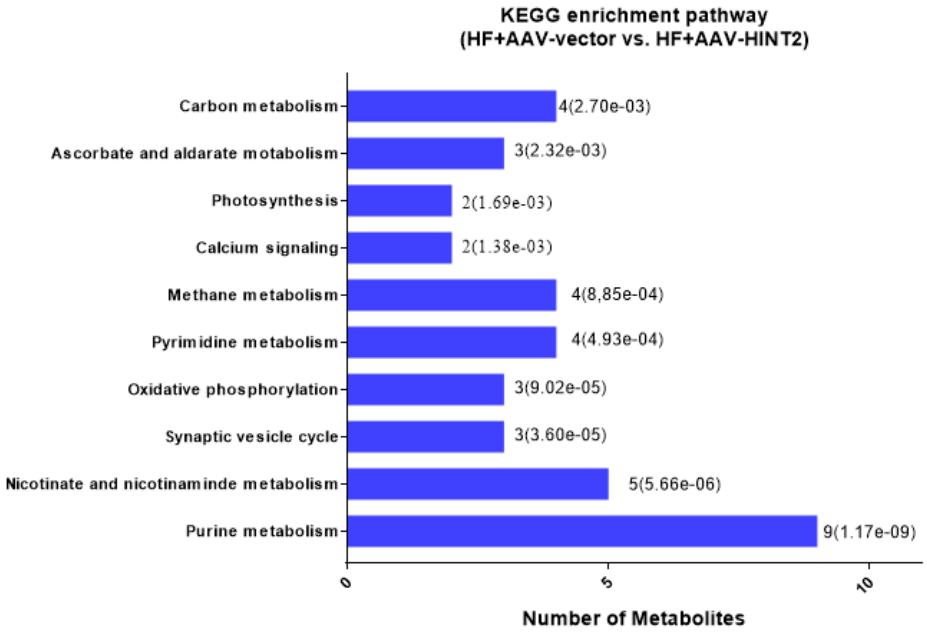

F

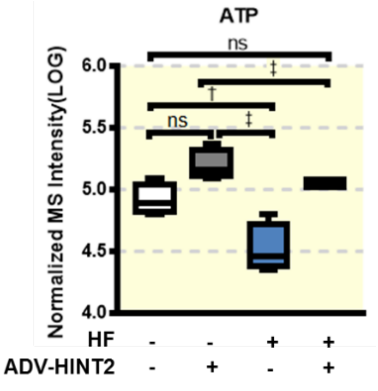

G

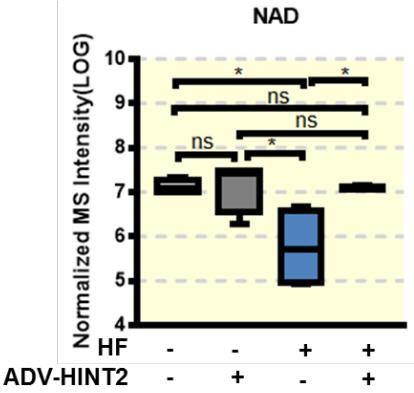

H

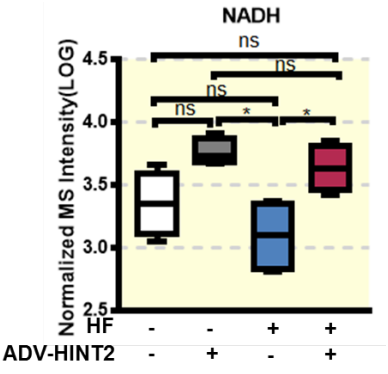

Figure 5

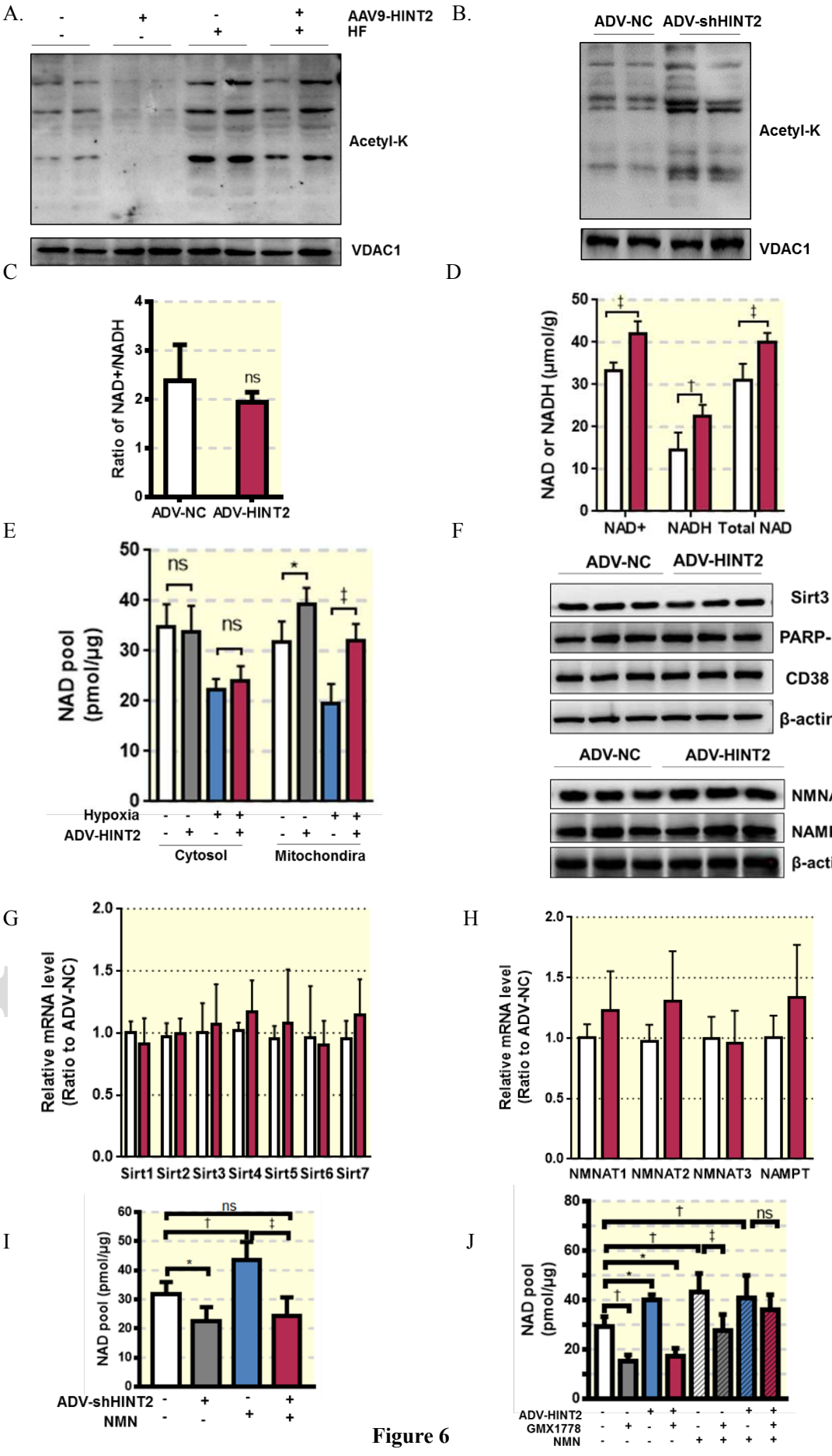

Figure 6

A

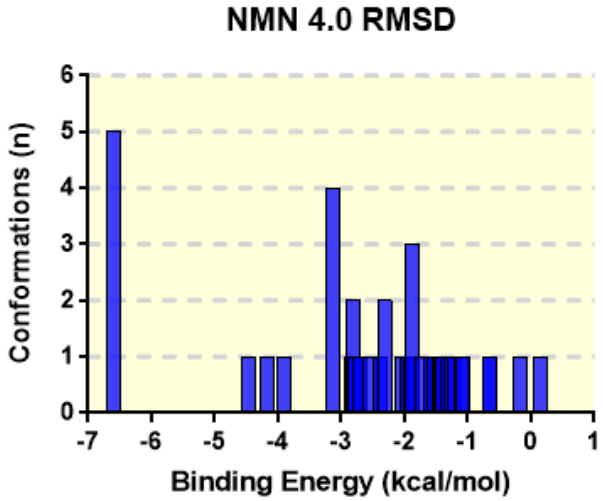

B

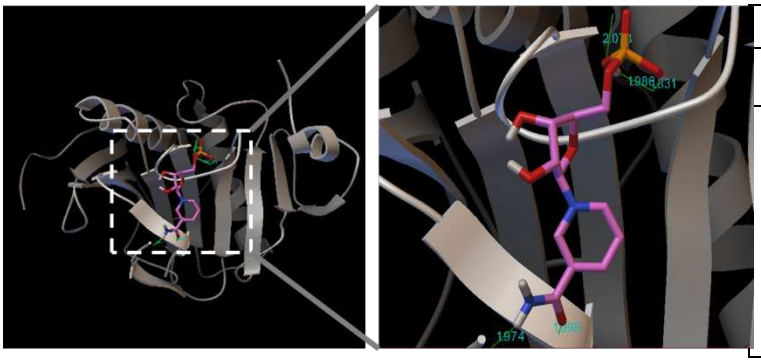

Binding energy:-6.6 kcal/mol
Inhibit constant: 14.63μM
5 hydrogen bonds formed:
NMN::UNL1:H: HIN2:B:GLN143:O
HINT2:A:TRP160:HN: NMN::UNL1:H:
HINT2:B:TYR146:HN NMN::UNL1:H:
NMN::UNL1:H: HIN2:A:GLN159:OE1
NMN::UNL1:H: HIN2:B:GLN143:O

C

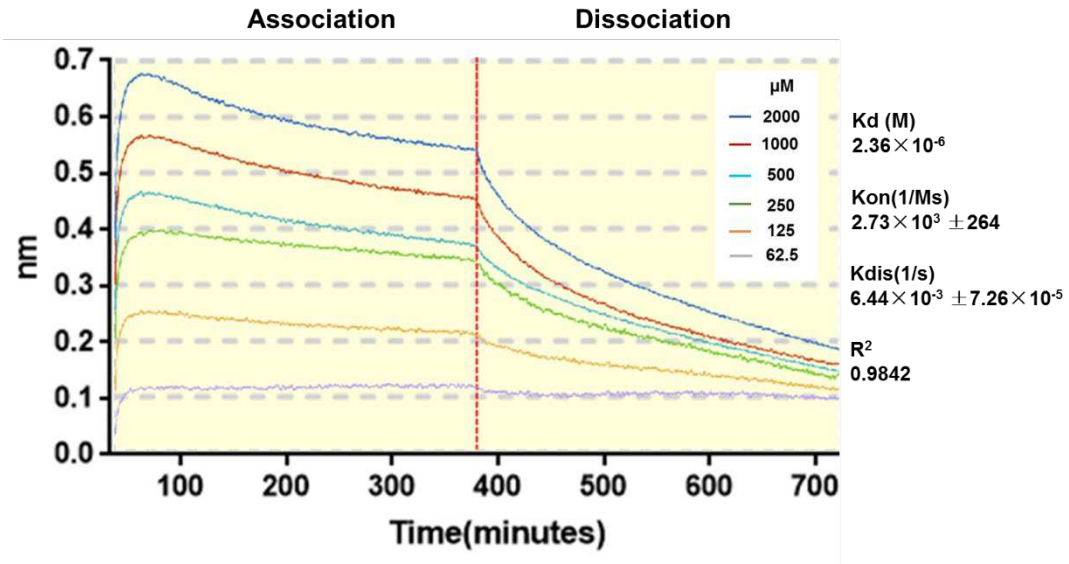

Figure 7